

We are IntechOpen, the world's leading publisher of Open Access books Built by scientists, for scientists

6,900

Open access books available

186,000

International authors and editors

200M

Downloads

Our authors are among the

154

Countries delivered to

TOP 1%

most cited scientists

12.2%

Contributors from top 500 universities



WEB OF SCIENCE™

Selection of our books indexed in the Book Citation Index
in Web of Science™ Core Collection (BKCI)

Interested in publishing with us?
Contact book.department@intechopen.com

Numbers displayed above are based on latest data collected.
For more information visit www.intechopen.com



Parametric Amplifiers in Optical Communication Systems: From Fundamentals to Applications

Jing Huang

Additional information is available at the end of the chapter

<http://dx.doi.org/10.5772/intechopen.73696>

Abstract

Optical parametric amplifiers (PAs) utilize highly efficient nonlinear effects in an optical fiber and they have the ability to operate in phase-sensitive mode. The inclusion of PAs in optical systems can give an ultimate limit for lumped amplified links in terms of achievable signal to noise ratio. The drawback is the complexity stemming from the requirement of phase matching a number of waves at each amplifier, phase lock, and the extra spectrum consumed by idler waves. In this chapter, the theories of a parametric amplifier, including the quantum-optical equations, are given. The properties of the gain saturation and the noise figure are presented. Practical amplifier systems and their applications in phase-sensitive amplification, all-optical signal regeneration, and squeeze state generation are outlined.

Keywords: four-wave mixing (FWM), modulation interaction (MI), gain, noise figure (NF), second harmonic generation (SHG), phase-sensitive amplification, parametric amplification

1. Introduction

Ultra-dense multi-channel transmissions at higher speed are required for the high capacity optical networks. These results in phase-based modulation such as binary and quadrature phase-shift keying (BPSK, QPSK) became increasingly interesting for optic communications in the years after 2000. And the application of optical parametric amplifiers (OPA) also becomes promising. The main reason for the current interest for parametric amplifiers is the ability to operate in phase-sensitive mode. Furthermore, OPA provides high gain (reaching to 10^4) and it can be used to handle high average powers. The drawback is the complexity

stemming from the requirement of phase matching a number of waves at each amplifier, and the extra spectrum consumed by idler waves [1].

In 1985, Pocholle et al. explored FWM for fiber-optic amplification [2]. The first phase-sensitive gain in an optical fiber was observed by Bar-Joseph et al. [3]. In 1993, Levenson et al. [4] observed the first optical amplification (in a KTP crystal) with a noise figure below the 3 dB limit. Marhic et al. [5] used a fiber Sagnac interferometer to realize parametric gain via degenerate FWM, and a similar structure was used by Imajuku et al. in 1999 [6], who reported the first $\chi^{(3)}$ -based parametric amplifier with a noise figure of 1.8 dB.

In parametric amplifiers, the stimulated Brillouin scattering (SBS) was suppressed by a broadband phase modulation of the pump. This pump phase modulation has some unwanted effects, such as idler spectral broadening and it is generally deleterious (but no fundamental obstacle) when realizing phase-sensitive amplifiers. However, such a fiber, with an induced strain gradient to suppress SBS, enabled phase-modulation-free CW pumping with 10 dB gain [7].

In 2005, Tang et al. [8] demonstrated phase-sensitive gain in a highly nonlinear fiber (HNLF) by first generating three phase-locked waves in a conventional phase-insensitive fiber-optic parametric amplifier (FOPA) and then injecting these into a second FOPA, which now became phase sensitive. The phase-sensitive nature was elegantly manifested as wavelength oscillations of the FOPA noise spectrum by inserting a dispersive fiber between the two FOPAs. This was the first realization of the copier-phase-sensitive amplifier (PSA) scheme. A number of important theoretical contributions to FOPAs and PSAs were published around this as well; notably by McKinstrie who analyzed phase-sensitive amplification classically [9] as well as quantum mechanically [10, 11]. Also, Marhic et al. contributed significantly, e.g., with work on the FOPA gain spectrum [12, 13]. Michel Marhic, who tragically passed away in 2014, also published the first book [14] on parametric fiber devices in 2008. In a series of papers by Croussore et al. [15–17], phase regenerators were realized and evaluated, being among the first PS devices to gain traction in the community. These were based on interferometric, degenerate parametric fiber devices.

The organization of this paper is as follows: Section 2 discusses fiber FWM from a fundamental perspective leading to the work on parametric amplifiers and the various flavors of these that exist; Section 3 presents the mathematical theory of FWM in fibers, Section 4 presents the 2-mode PSA and the coherent superposition; and Section 5 describes the PSA noise properties, both from a semi-classical and a quantum mechanical perspective, and gain saturation properties. At the last parts, the copier-PSA setup that has been used in experiments including the polarization properties and nonlinear tolerance, the practical systems of parametric amplifier, and their applications are introduced.

2. Fiber optic parametric amplifier theory

In fibers, the refractive index is a function of the light intensity. If two waves (ω_1 and ω_2) copropagate in a medium, they will interfere and create a moving grating, and a third wave ω_3 may scatter, and then a fourth wave at ω_4 may generate. This is named as four-wave

mixing. The fourth wave will be generated at a frequency which is the Doppler-shifted from scattering wave, $\omega_4 = \omega_3 + \omega_2 - \omega_1$. For the process to be efficient, the corresponding Bragg condition $\beta_4 = \beta_3 + \beta_2 - \beta_1$ must also be satisfied, where β_k is the propagation constants of wave k . This is also commonly referred to as the phase-matching condition. Note that both the Doppler and Bragg conditions need to be fulfilled for FWM to be efficient, and for a given dispersion relation $\beta(\omega)$, both conditions are not generally satisfied. However, around the zero-dispersion wavelength they are. This is the classical picture of FWM, and it is also very useful in understanding the polarization properties.

Light propagation in optical fibers is remarkably well described by the nonlinear Schrodinger Equation (NLSE), in a slightly generalized form with all dispersive orders as

$$i \frac{\partial u}{\partial z} + \beta \left(\omega_0 - i \frac{\partial}{\partial t} \right) u + \gamma |u|^2 u = 0 \quad (1)$$

where $\beta(\omega)$ is the dispersion relation of the fiber, ω_0 is the carrier frequency, the independent variable z is the fiber length, and the local time is t . As written, $\beta(\omega_0 - i\partial/\partial t)$ should be interpreted as a differential operator, defined by the Taylor expansion of β around ω_0 . The field amplitude $u(z, t)$ is chosen so that $|u|^2$ is the propagated power in Watt units. The nonlinear coefficient γ is around 15 (W km)^{-1} for HNLFs. Losses are neglected as the propagation is only over a few 100 m of HNLF.

Consider the propagation of three waves, a pump symmetrically surrounded by a signal and an idler wave, i.e., $u = u_p \exp(i\omega_p t) + u_s \exp(i\omega_s t) + u_i \exp(i\omega_i t)$, where $2\omega_p = \omega_i + \omega_s$. We assume CWs, so that $u_{p,s,i}(z)$ are the functions of z only. After inserting this into the NLSE, we collect terms oscillating at the three separate frequencies and neglect the others. The result is the coupled system

$$\frac{\partial u_p}{\partial z} = i u_p \left[\beta_p + \gamma (2P - |u_p|^2) \right] + i \gamma 2 u_p^* u_s u_i \quad (2)$$

$$\frac{\partial u_s}{\partial z} = i u_s \left[\beta_s + \gamma (2P - |u_s|^2) \right] + i \gamma 2 u_p^2 u_i^* \quad (3)$$

$$\frac{\partial u_i}{\partial z} = i u_i \left[\beta_i + \gamma (2P - |u_i|^2) \right] + i \gamma 2 u_p^2 u_s^* \quad (4)$$

$P = |u_s|^2 + |u_p|^2 + |u_i|^2$ is the total power.

The pump power is much larger than the signal power, i.e., $|u_p|^2 = P_p \gg |u_{s,i}|^2$. Then (2) for the pump can be approximately solved as $u_p(z) = \sqrt{P_p} \exp[i(\beta_p + \gamma P_p)z]$. After inserting this into (3) and (4) and peeling off the phase via the substitution $u_{s,i} = e_{s,i} \exp(i(\kappa + \beta_{s,i})z)$, one has a coupled first-order system with constant coefficients as

$$\frac{de_s}{dz} = i \kappa e_s + i \gamma P_p e_i^* \quad (5)$$

$$\frac{de_i^*}{dz} = -i \kappa e_i^* - i \gamma P_p e_s \quad (6)$$

Here, we introduced the notation $\kappa = \gamma P_p + \Delta\beta/2$, where $\Delta\beta = 2\beta_p - \beta_s - \beta_i$ is the linear phase mismatch. In matrix form

$$\frac{d}{dz} \vec{E}(z) = i \begin{vmatrix} \kappa & \gamma P_p \\ -\gamma P_p & -\kappa \end{vmatrix} \vec{E} = M \vec{E} \quad (7)$$

where M is the coefficient matrix and $\vec{E}(z) = \begin{vmatrix} e_s(z) \\ e_i^*(z) \end{vmatrix}$. A convenient way is to use the matrix exponential, to write the solution as

$$\vec{E}(z) = \exp(iMz) \vec{E}(0) = K(z) \vec{E}(0) \quad (8)$$

The transfer matrix $K(z)$ can be explicitly expressed as

$$K = I \cosh(gz) + iM \frac{\sinh(gz)}{g} \\ = \begin{vmatrix} \cosh(gz) + i\frac{\kappa}{g} \sinh(gz) & i\frac{\gamma P_p}{g} \sinh(gz) \\ i\frac{\gamma}{g} \sinh(gz) & \cosh(gz) - i\frac{\kappa}{g} \sinh(gz) \end{vmatrix} \quad (9)$$

Here, $g = (\gamma P_p)^2 - \kappa^2$ is the parametric gain coefficient, which is maximum when κ vanishes, and this occurs when the linear mismatch balances the nonlinear phase shift.

The maximum parametric gain (for $\kappa = 0$) equals $G = \cosh^2(\gamma P_p z)$, and it is the phase-insensitive gain, since it is the gain the signal wave gets when no idler is present at the input. It grows exponentially with the nonlinear phase shift $\gamma P_p z$. If the pump lies exactly on the zero-dispersion frequency, the linear mismatch $\Delta\beta$ vanishes, and the transfer matrix reduces to

$$K = I + iMz = \begin{vmatrix} 1 + i\gamma P_p z & i\gamma P_p z \\ -i\gamma P_p z & 1 - i\gamma P_p z \end{vmatrix} \quad (10)$$

which is linear in the nonlinear phase shift. The corresponding parametric gain is quadratic in the nonlinear phase shift. However, this scheme has theoretically very large bandwidth that in practice will be limited by longitudinal zero-dispersion variations [18, 19] and/or higher orders of dispersion [12].

The properties of the transfer matrix K are important in order to understand and explain the gain and noise properties of parametric amplifiers. It is often given in a general form as

$$K = \begin{vmatrix} \mu & \nu \\ \nu^* & \mu^* \end{vmatrix} \quad (11)$$

where μ and ν are complex coefficients, so that $|\mu|^2 - |\nu|^2 = 1$.

Eq. (11) parameterizes the set of matrices that preserve the invariant. Matrices with this property form a group, the symplectic group, which means that the product of two symplectic matrices is

also symplectic. It is interesting to compare and contrast with the unitary group, which preserve the sum of the powers (rather than the difference) and has a similar (but not equivalent) parameterization. The symplectic property was discussed for parametric processes in [20].

By inspection of the form of K in (11), we can draw some important conclusions. The phase-insensitive gain is $G = |\mu|^2$ and the idler conversion efficiency is $\eta = |v|^2 = G - 1$. The absolute phases of the μ and v coefficients are mostly of less interest, and in many cases, it is enough to characterize the transfer matrix by the single parameter G .

3. Phase-sensitive parametric amplifier

If both waves (signal and idler) are present at the input, the interaction given by the matrix K above is phase sensitive, i.e., the two waves $e_{s,in}$ and $e_{i,in}$ will be coherently superposed, as in interferometry, so the corresponding output waves will be

$$e_{s,out} = \mu e_{s,in} + v e_{i,in}^* \quad (12)$$

$$e_{i,out}^* = v^* e_{i,in}^* + \mu^* e_{s,in} \quad (13)$$

In reality this is difficult to realize as it requires phase-locking between the pump, signal, and idler waves. The three waves can be generated by either using a “copier,” as done originally by Tang et al. [8] or by using phase-locked frequency lines from a single laser source by, e.g., external modulation, as used in the work by Bar-Joseph et al. [3].

We see directly from the transfer equations that a two-mode PSA with equal signal and idler powers will experience a phase dependent gain for the signal as

$$G_{PSA} = \frac{|e_s \mu + e_i^* v|^2}{|e_s|^2} \quad (14)$$

For equal input signal and idler powers, this can be written

$$G_{PSA}(\phi) = |\mu|^2 + |v|^2 + 2|\mu||v| \cos(\phi) \quad (15)$$

where ϕ is the phase angle of $\mu e_s v^* e_i^*$, which we can interpret as the phase difference $\phi = \phi_s + \phi_i - 2\phi_p$ between the pump and signal waves entering the amplifier. We can take the pump phase to be zero, which is of no restriction. Clearly, this gain is maximum (minimum) for $\phi = 0$ ($\phi = \pi$). It is straightforward to show that the maximum and minimum phase-sensitive gains are reciprocal, i.e., $G_{max/min} = (|\mu| \pm |v|)^2 = \exp(\pm 2\gamma P_p z)$. In a degenerate PSA, where the idler and the signal are the same, $\phi = 2\phi_s$, and then one quadrature $\phi_s = 0$ of the signal will exhibit gain and the other $\phi_s = \pi/2$ will exhibit anti-gain (or parametric loss). In other words, one quadrature is parametrically amplified, and the other is attenuated the same amount. This has also been clearly verified experimentally. The phase modulation applied to the pump, used to suppress SBS, reduces fidelity in such experiments by limiting the parametric attenuation, but phase-sensitive gains of up to 30 dB have been observed [21].

It is also notable that in the high-gain regime $\mu \approx \nu \approx \sqrt{G}$, and the $G_{max} = G_{PSA}(0) \approx 4|\mu|^2 = 4G$, there is 6dB difference between the phase-sensitive and phase-insensitive gain. This is due to the coherent superposition of two waves, and it can be generalized to give N^2 -fold increase for an N -mode amplifier. For example the 4-mode PSA, the PS gain is 16 times of the PI. In the corresponding experiment, 10.5 dB was measured [22].

The specific eigenmodes that are amplified/attenuated may differ in various systems. For example, in the 2-mode amplifier, there can be linear combinations so that $e_s + e_i^*$ exhibits gain and $e_s - e_i^*$ exhibits loss. By decomposing the transfer matrix into a matrix product whose elements are defined by its eigenmodes and eigenvalues (i.e., singular value decomposition, but in this context called Schmidt decomposition and Schmidt modes), one can gain further insight into multimode phase-sensitive processes [23].

4. Saturation gain of parametric amplifier

When power is transferred from the pump to the signal, the optical-pump power cannot sustain the exponential growth of the gain, saturation occurs [24]. The relative magnitudes of the pump and signal/idler powers will affect the flow of power between them due to the nonlinear phase-matching condition.

The asymptotic power conversion corresponds to a gain that can be expressed as

$$G(P_{s0}) = \frac{G_0}{1 + P_{s0}/P_{sat}} \quad (16)$$

where G_0 is the unsaturated gain given by

$$G_0 = 1 + \frac{16}{7} \sinh^2 \left(\frac{\sqrt{7}}{4} \gamma P_p L \right) \quad (17)$$

and P_{s0} is the signal input power. The saturation power P_{sat} is given by

$$P_{sat} = \frac{1}{2} \frac{P_p}{G_0} \quad (18)$$

This saturation power can be interpreted as the input signal power required for the gain G_0 to convert the whole pump to the signal and idler waves. These equations are only valid for the single wavelength when the pump is totally converted and under the assumption of three waves only.

In **Figure 1**, the gain spectrum as a function of λ_n for different signal input powers are plotted. Here, $\lambda_n = (\lambda_s - \lambda_p)/(\lambda_{max} - \lambda_p)$ is the signal wavelength normalized so that $\lambda_n = 1$ corresponds to the maximum gain wavelength λ_{max} , $\lambda_n = 1/2$ is the asymptotic conversion wavelength, and $\lambda_n = 0$ is the pump wavelength.

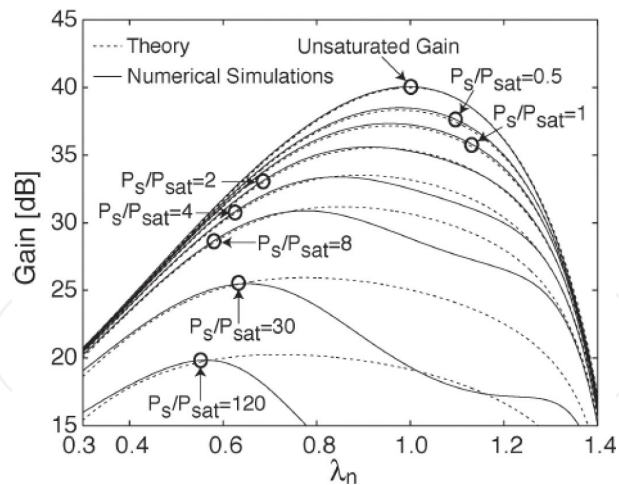


Figure 1. Gain spectrum as a function of λ_n for different signal input powers. P_{s0} is normalized to the saturation power at the gain peak $P_{sat,max}$, P_{s0}/P_{sat} . The peak gain is 40 dB, and $P_{s0}/P_{sat,max} = 0$ (unsaturated gain), 0.50, 1, 2, 4, 8, 30, and 120.

The signal input powers are normalized to the saturated gain at the gain-peak wavelength according to $P_{s0}/P_{sat,max}$. As the input power increases, the peak gain shifts toward the pump wavelength, because the nonlinear phase matching is altered as the signal/idler powers increase. The pump is completely converted at $\lambda_n = 0.5$. The peak gain is shifted to that wavelength of higher input power and at other wavelengths, the power is periodically exchanged between the signal/idler and optical pump with length. This also explains the dramatic change in gain which is reduced at higher normalized input powers.

5. Noise in amplifiers

This section will discuss the noise properties of parametric amplifiers and in particular PSAs. We will consider both the semi-classical approach and the quantum mechanical.

5.1. Semi-classical model

The semi-classical model of light-matter interaction means that one has a classical field formulation, but a quantum mechanical model of matter. When modeling noise in optical amplification, the amplifier has spontaneously emitted photons that can be treated as additive noise and that have (at the amplifier input) a power spectral density of half a photon per mode.

From this assumption, a lot of well-known results follow; for example, the shot noise power spectral density and the familiar result for amplifier noise figures. The NF is defined as the ratio of input to output SNR (in the electrical domain, after ideal photodetection) of an optical amplifier. It is also a measure of the amount of spontaneous emission noise an amplifier adds to a signal.

Phase-insensitive amplifiers (PIA) have a noise figure of $NF_{PIA} = 2 - 1/G$, approaching 3 dB for high gain. Parametric amplifiers have, in phase-sensitive operation, a noise figure of $NF_{PSA} = 1$

(gain is 0 dB) instead, because the quantum noise is unevenly between the adjoining quadratures (which is known as squeezing). The PSA, however, have a NF of 1/2 (−3 dB) if only the signal wave is considered and the idler contains a conjugate signal copy. This comes from the 6 dB difference in gain between PIA and PSA as we saw above and ultimately from the coherent superposition. This means that a PSA and a PIA giving the same gain will have ASE noise floors that differ by 6 dB, as shown in the measured optical spectrum in **Figure 2**. More detailed derivations based on the semi-classical approach can be found in [25].

5.2. Quantum theory

A full noise theory for the PSA must be based on quantum mechanics, and we sketch a derivation here [26]. In quantum field theory, the two quadratures of a mode are described by operators $a_{1,2}$ that must obey the commutator relation $[a_1, a_2] = i/2$. The commutation between two operators implies a Heisenberg uncertainty relation between the two modes. A linear amplifier with gain $G_{1,2}$ for the respective quadratures is described by

$$b_1 = \sqrt{G_1}a_1 + F_1 \quad (19)$$

$$b_2 = \sqrt{G_2}a_2 + F_2 \quad (20)$$

where the added noise field operators $F_{1,2}$ are necessary if the commutation relation should hold also for the output modes $b_{1,2}$. It is easy to see that the absence of these noise fields would lead to contradictions, e.g., arbitrarily small uncertainties violating the Heisenberg uncertainty relation. Thus, every amplifier must have these additive fields. Applying the commutation relation to the output fields gives a relation on the noise field operators as

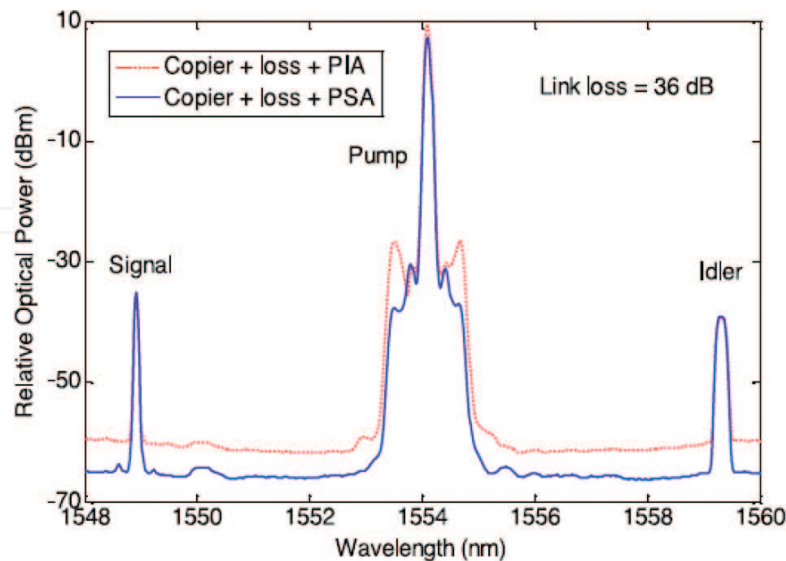


Figure 2. Optical spectra of a 2-mode parametric amplifier in PS and PI modes. The pump in the PI case is higher to make the gain equal, which leads to 6 dB higher noise floor for the PIA [25]. The increased noise close to the pumps for the PIA is likely due to dispersion variations along the HNLF, making these frequencies phase matched and having higher gain in some portions of the fiber.

$$[F_1, F_2] = \frac{i}{2} \left(1 - \sqrt{G_1 G_2}\right) \quad (21)$$

The Robertson uncertainty relation states that if two operators commute with a commutator x , their uncertainty product is $|x|^2$. The uncertainty for $F_{1,2}$ is then

$$\langle \Delta F_1^2 \Delta F_2^2 \rangle = \frac{1}{4} \left(1 - \sqrt{G_1 G_2}\right)^2 \quad (22)$$

The noise figure is then

$$\begin{aligned} NF_{PSA} &= \frac{\langle a_1^2 \rangle \langle a_2^2 \rangle \langle \Delta b_1^2 \rangle \langle \Delta b_2^2 \rangle}{\langle \Delta a_1^2 \rangle \langle \Delta a_2^2 \rangle \langle b_1^2 \rangle \langle b_2^2 \rangle} \\ &= 1 + \frac{\langle \Delta F_1^2 \Delta F_2^2 \rangle \langle \Delta b_2^2 \rangle}{G_1 G_2 \langle \Delta a_1^2 \rangle \langle \Delta a_2^2 \rangle} \\ &= 1 + \left(1 - \frac{1}{\sqrt{G_1 G_2}}\right)^2 \end{aligned} \quad (23)$$

For a PSA, the two quadratures' gain obey $G_1 G_2 = 1$, and this then reduces to $NF_{PSA} = 1$. For the PIA, $G_1 = G_2 = G$, and the derivation can be simplified by noting that the gain is the same for both quadratures, so that

$$NF_{PIA} = 1 + \frac{\langle \Delta F^2 \rangle}{G \langle \Delta a^2 \rangle} = 1 + \left(1 - \frac{1}{G}\right) = 2 - \frac{1}{G} \quad (24)$$

This summarizes the well-known properties of the noise figures for amplifiers. More detailed discussions on the quantum mechanical properties of parametric processes (including, for example, the noise for the phase conjugation and Bragg scattering processes) can be found in the works of McKinstrie [10, 11].

It should also be mentioned that other noise sources than the fundamental quantum noise discussed above contribute to parametric amplifiers, e.g., noise from the Raman effect, pump-induced noise, and excess ASE noise from the pump boosters which can make it difficult to get closer than 1 dB within the quantum noise figure limit in experiments.

6. Several kinds of parametric amplifiers

6.1. Basic setup

The most convenient PAs for use at communication wavelengths are based on nonlinear interferometers (NIs) or operate directly in fiber through partially degenerate FWM, which are listed in **Figures 3** and **4** [27, 28].

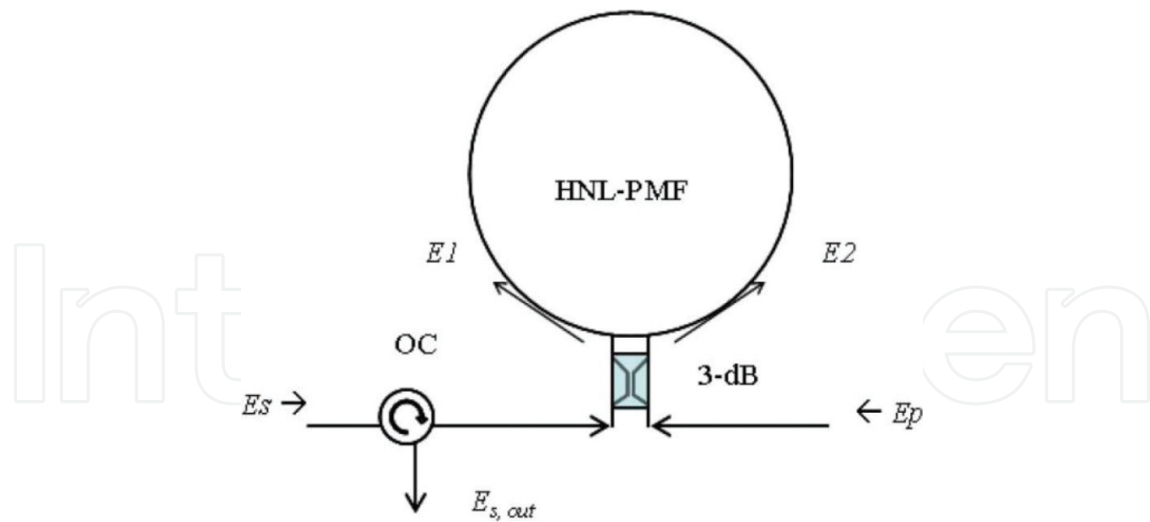


Figure 3. NI-PSA based on a Sagnac interferometer and optical fiber. OC: optical circulator; PC: PM/AM: noise adding phase and amplitude modulators.

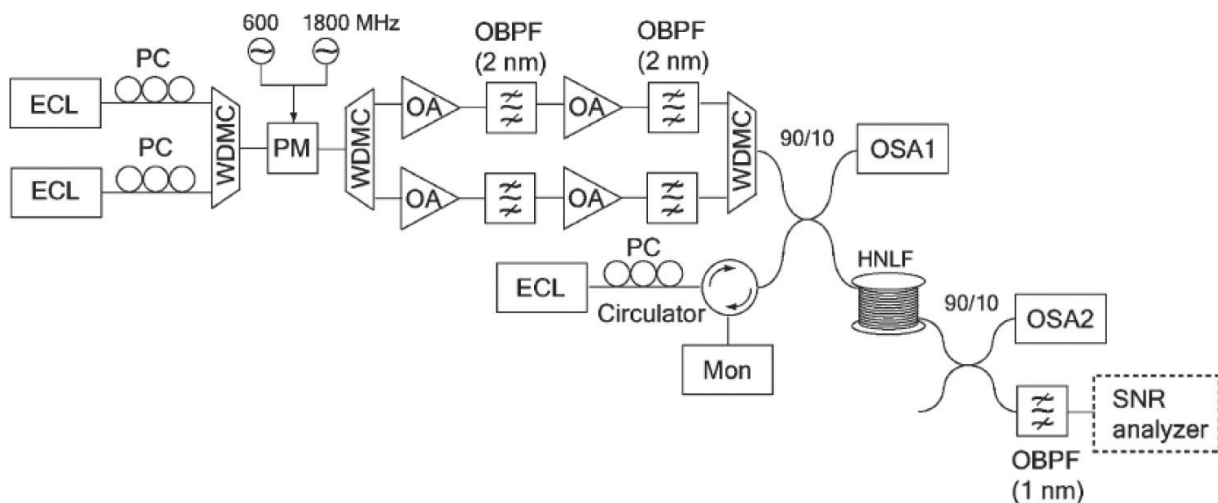


Figure 4. Setup of parametric amplification. ECL: external cavity laser, PC: polarization controller, WDMC: wavelength division multiplexing coupler, PM: phase modulator, OA: optical amplifier, OBPF: optical bandpass filter, OSA: optical spectrum analyzer, HNLf: highly nonlinear fiber, and Mon: optical power monitor.

An example of a Sagnac interferometer is depicted in **Figure 3**. Phase sensitivity of the gain arises from the interference of the waves at the input and output combined with nonlinear phase shifts due to SPM [27].

A 2-pump PA with a gain bandwidth of approximately 25 nm is shown in **Figure 4**. A method based on lock-in amplification is used. The two pumps (wavelengths $\lambda_C = 1563$ nm and $\lambda_L = 1600$ nm) are placed roughly symmetrically around the zero-dispersion wavelength, $\lambda_0 = 1582$ nm. The length of HNLf is $L = 520$ m and nonlinearity parameter is $\gamma \approx 16/\text{W}/\text{km}$. The pump powers are provided by external cavity lasers (ECLs), combined with low-loss wavelength division multiplexing couplers (WDMCs) and sent into a phase modulator (PM). Two radio frequencies (RFs) 600 and 1800 MHz are sent to the PM to reduce the SBS. The high

frequencies of the PM are necessary because the PM produces gain fluctuations, which create discrete frequency harmonics in the electrical spectrum of the detected signal. The two pumps are combined after the PM and amplified by two erbium-doped fiber amplifiers (EDFAs). The pumps are then filtered and boosted by high-power EDFAs, and filtered again by 2 nm optical bandpass filters (OBPFs). They are finally combined with the signal and launched into the HNLF. An optical spectrum analyzer (OSA) monitored the input powers of the signal and pumps. Another OSA monitors the output powers. The signal is filtered by an OBPF before sent to the SNR analyzer.

6.2. Optical parametric chirped-pulse amplifier system

Optical parametric chirped-pulse amplification (OPCPA) is an efficient way to amplify short optical pulses to high-power levels while avoiding some of the pitfalls of conventional CPA systems, specifically, gain narrowing, unwanted nonlinearities, and thermal effects [29].

The system includes the 1.064 μm pump laser, the tunable 1.6 μm fiber seed laser, the timing electronics setups, the rubidium titanyl phosphate (RTP) and potassium titanyl arsenate (KTA) (as the OPA crystals), and the stretcher and compressor. The timing circuitry is used to lock the phase of the two seed oscillators.

The layout of the system is shown in **Figure 5**. A 40 MHz fiber laser and amplifier provide the signal pulse and act as the master clock for the system. The custom-built fiber system is based on the design given in [30]. The short pulse (<100 fs) is used as a signal source that can tune the OPCPA across the range from 1500 to 1650 nm. These pulses are stretched to 300 ps in a stretcher (a 600 line/mm grating); however, due to the bandwidth limitations in the OPA

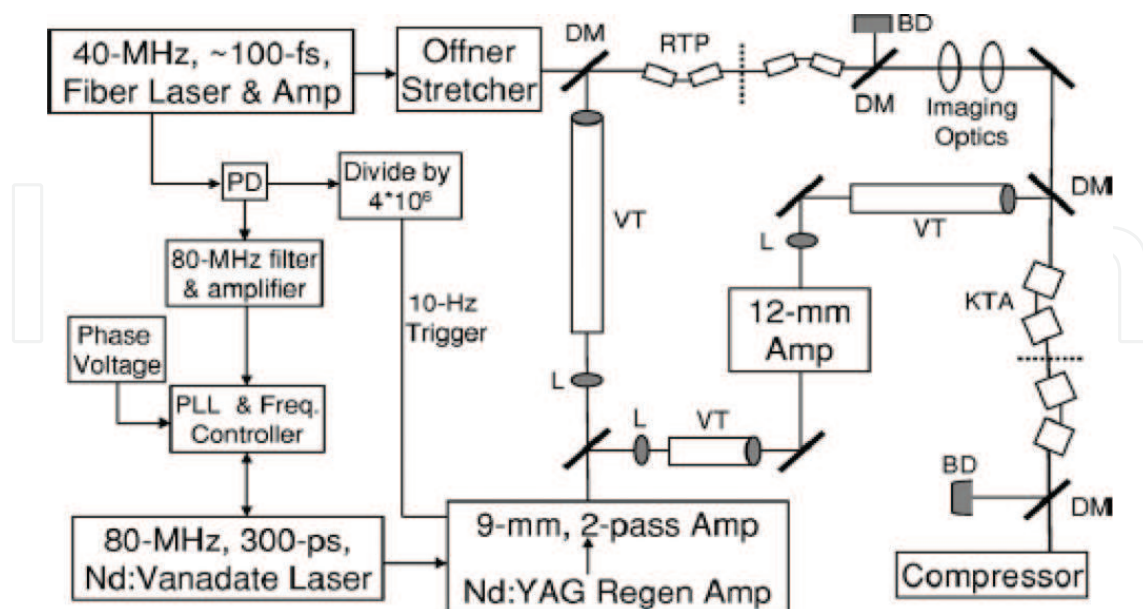


Figure 5. The system's optical and electric control layout. Dotted lines are image planes for the relay. RTP and KTA are the nonlinear crystals. VT, vacuum tubes; L, relay imaging lens; PD, photodiode; DM, dichroic mirror; and BD, beam dump.

crystals (only 10–20 nm are amplified). This reduced the bandwidth of the pulse (stretched only 30–60 ps).

The 40 MHz photodiode signal generated the 80 MHz harmonic, then filtered, and amplified the input of the phase-locked loop (PLL) to stabilize the 80 MHz pump seed laser. The seed laser is a 300 ps mode-locked Nd:vanadate laser that uses a semiconductor saturable absorber and mirror mode locker. The cavity length is controlled by a motor to maintain the repetition rate and to rapidly compensate the mechanical instabilities. The laser and locker reduce the relative timing jitter between the two lasers (<2 ps rms over the 1–100 kHz frequency range), and the piezo inducing jitter (<1 ps rms for frequencies less than 1 kHz). By employing this timing stabilization technique, the OPCPA has the ability to accept any signal that its repetition rate is some integer fraction of the 80 MHz pump laser. Once the two lasers are frequency locked, the relative phase shift between the pump and the signal pulses is set to within ± 1 ns by inserting the proper electrical equipment between the 80 MHz clock signal and the PLL. The phase voltage can adjust the relative phase of the pulses at a rate of 60 ps/V. As shown in **Figure 8**, a separate output from the photodiode is transferred to 10 Hz by the standard digital electronics and then acts as the trigger for both the flash lamps and the Pockels cells in the Nd:YAG amplifier chain.

The first stage of this chain is a regeneration amplifier (the 10 nJ seed pulse to 40 mJ). The output is then collimated and amplified to 375 mJ in Nd:YAG and two-pass power amplifiers.

A software is designed to model nonlinear optical interactions. The 1.6 μm broadband light is amplified by a 1.064 μm monochromatic pump in a collinear configuration. Both crystals, RTP and KTA, have broad phase-matched bandwidths in the 1.5–1.6 μm region when used in a collinear geometry, and each has a d_{eff} between 2 and 2.5 pm/V for the optical parametric amplification process. The system uses four $5 \times 5 \times 6$ mm RTP crystals as the preamplifiers since its bandwidth and gain are superior to KTA; however, RTP absorbs 25% of the idler energy and its aperture cannot be manufactured large enough to act as a power amplifier. For these reasons, four $8 \times 8 \times 8$ KTA crystals are used as the power amplifiers. The spatial walk-off between the signal and the pump beams is compensated. The four-crystal arrangement provides uniform gain across the signal beam.

6.3. Tunable single-longitudinal mode fiber optical parametric oscillator (SLM FOPO)

A sub-ring cavity with a short length is used to suppress the longitudinal modes and broaden the longitudinal mode spacing [31]. A fiber loop mirror, consisted of an unpumped erbium-doped fiber, acts as an auto-tracking filter to ensure the single frequency operation. The measurement shows that the FOPO has the SLM output. It can be tunable over 14 nm for each of the signal and idler, which is limited only by the gain bandwidth of parametric amplifier.

In **Figure 6**, the pump is seeded by an external cavity tunable laser source (TLS) at the wavelength 1556 nm. To suppress the stimulated SBS, the light from the TLS is modulated with a 10 Gb/s pseudorandom bit sequence signal via a phase modulator (PM). A polarization controller PC1 aligns the polarization state of pump with the axis of the PM. The SBS can be suppressed up to 28 dB. Then the pump is amplified by a two stage EDFA, in which the first

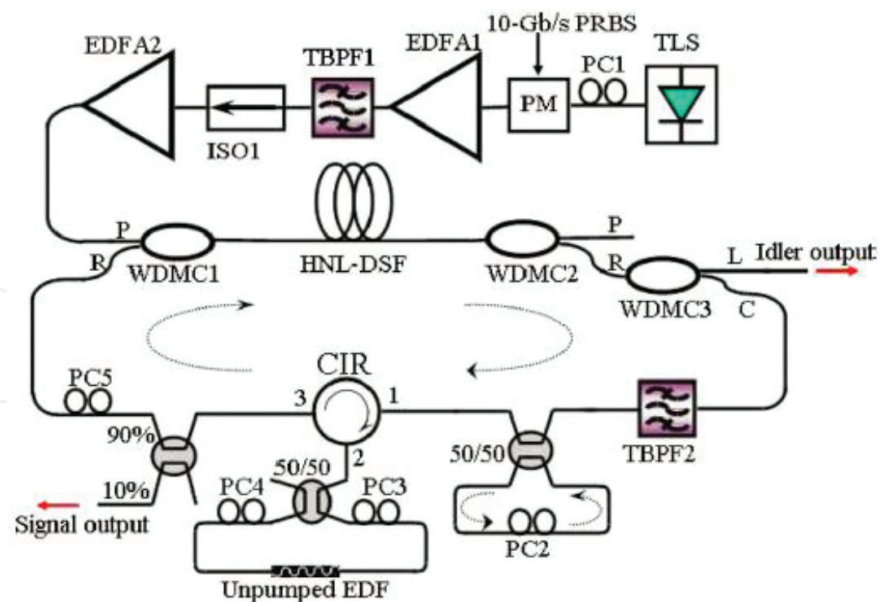


Figure 6. Schematic diagram of the tunable SLM FOPO.

stage (EDFA1) provides small signal gain to prevent self-saturation. The 0.35 nm tunable bandpass filter (TBPF1) is used to reduce the ASE noise. After passing through an isolator (ISO1), the pump is further amplified by the second stage (EDFA2), with a maximum output power of 33 dBm. Then the pump is coupled into a 400 m highly nonlinear dispersion-shifted fiber (HNL-DSF) with the zero-dispersion wavelength at 1554 nm via the P-port (transmission band: 1554.89–1563.89 nm) of a WDM coupler (WDMC1). The high-power pump is then rejected through the P-port of another WDMC2, while the amplified signal and idler propagate first through the R-port (reflection bands: 1500–1551 and 1567–1620 nm) of WDMC2 and subsequently are split into two paths by a C/L band WDMC3. Only the signal is coupled into the cavity and can oscillate, while the idler is coupled out through the L-port of WDMC3. The signal from the C-port of WDMC3 is filtered by 0.35 nm TBPF2, which determines the lasing wavelength and the possible oscillation modes. The cavity with length about 4.1 m is then inserted after TBPF2. It consists of a PC and a 50/50 coupler. Subsequently, a fiber loop mirror is linked via an optical circulator. The loop mirror consists of a 50/50 coupler, two PCs (PC3 and PC4), and a 3.5 m unpumped EDF that serves as the saturable absorber. The two in-line PCs (PC3 and PC4) are used to control the polarization state of the light. A 10/90 optical coupler is used to couple out 10% of the signal light. PC5 is used to align the polarization of the signal with the pump so as to maximize the signal gain.

The resonant frequencies of the ring cavities are obtained by making the total phase shift along the ring path equals an integral multiple of 2π . The longitudinal mode spacing is $\Delta\nu = c/nL$, in which c is the light speed in vacuum, n is the refractive index of the ring, and L is the cavity length. So the longitudinal mode spacing is the inverse ratio of the cavity length. To suppress the longitudinal modes and increase the longitudinal mode spacing, a coupled sub-ring cavity with a short cavity length is deployed as a mode filter. The longitudinal mode spacing can be increased from kilo-Hz level to mega-Hz level by this method. The second mechanism is a

fiber loop mirror with an unpumped EDF. In the fiber loop mirror, two counter-propagating waves form a standing wave and induce spatial hole burning (SHB) in the unpumped EDF. The refraction index of the EDF changes spatially and results in an ultra-narrow bandwidth self-induced fiber Bragg grating (FBG). After the fiber loop mirror, only SLM can be transmitted and oscillated.

7. The copier-phase-sensitive amplifier

A powerful way to realize a PSA transmission link is to generate the idler wave in a parametric amplifier as a “copier” [32, 33] as shown in **Figure 7**. Then the pump, signal and idler waves will be automatically phase locked. This means that an arbitrary modulated signal can be phase-sensitively amplified along the link if all three waves are transmitted, and also, that several signal wavelengths can be used with their corresponding idlers and pump. Three channels with QPSK modulation are amplified by a 20 dB PSA using this scheme.

7.1. Sensitivity improvement

In order to obtain the 6 dB of SNR improvement for the copier-PSA scheme, it is important that the noise at the signal and idler wavelengths are uncorrelated [33], which is accomplished by the attenuation after the copier. The end result is, however, that the copier-PSA link gets a 4-fold increase of the transmission distance, at the expense of using twice the bandwidth, as the same data occupies both the signal and the idler wavelengths [34].

7.2. Nonlinear compensation

The copier-PSA scheme has one additional, somewhat unexpected, benefit over schemes that does not co-transmit a conjugated idler wave. That is, its ability to compensate nonlinear distortions from, e.g., self-phase modulation or nonlinear phase noise. The principle is similar to the so-called phase-conjugated twin waves [35], where the idea is to transmit the data and the conjugate data on two parallel channels.

When the two channels are superposed in digital signal processing, the nonlinear distortions will cancel out (to first order). In the copier-PSA scheme, the exact same superposition takes

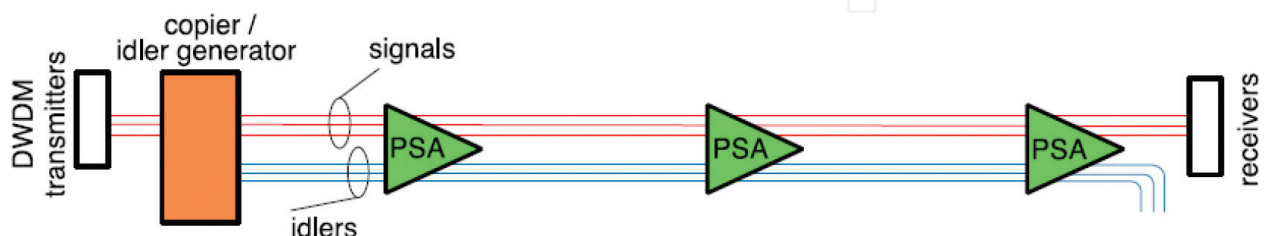


Figure 7. Transmission system based on the copier-PSA scheme. A copier (a PI parametric amplifier) directly after the transmitter generates idler waves that are conjugated versions of the signals. The idlers are only used as internal modes and dropped before detection.

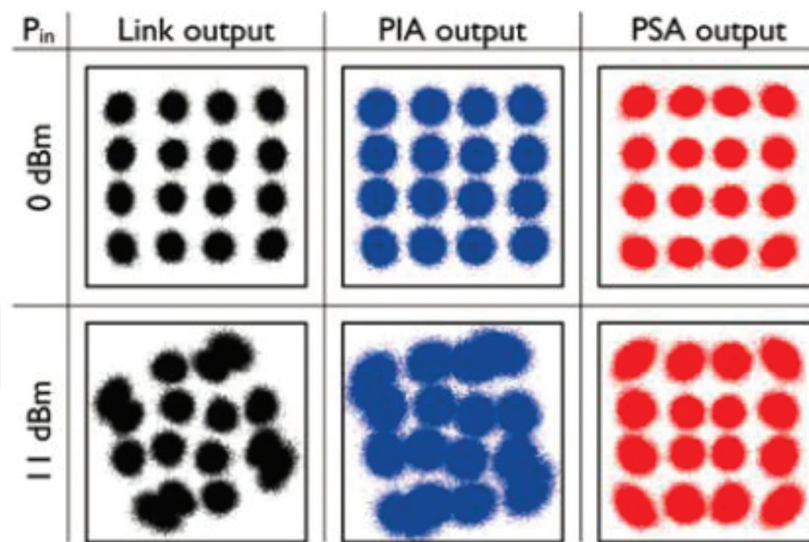


Figure 8. Linear (upper row) and nonlinear (lower row) transmission of 16-QAM data through a link and after amplification with PIA or PSA.

place in the PSA and significant nonlinear suppression can be seen. An example of a measured 16-quadrature amplitude modulation (QAM) constellation is shown in **Figure 8**.

7.3. Experimental system

The experimental setup is shown in **Figure 10** [36]. A continuous wave laser (200 kHz linewidth) at 1549.5 nm is modulated by 10 GBd 16QAM data in an IQ-modulator and then combined with a 28 dBm CW pump at 1553.7 nm in a WDM coupler.

The waves are launched into the copier (HNLF) and the net conversion efficiency is about -5 dB. An idler wave is generated at 1557.5 nm. The pump wave is then attenuated for 4 dBm power in the variable optical attenuator (VOA), VOA1, and passes through an optical delay line for equalization of the optical path between the copier and the PSA. The signal and idler waves pass through an optical processor for delay and amplitude tuning. The waves are tuned so that they have the same timing and amplitude at the PSA input. The optical processor is also used for switching between phase-insensitive (PI) and PS operation by either blocking or letting through the idler wave.

After re-combining the three waves, they are launched into a DCF for pre-compensation (dispersion is equivalent to 23.6 km of SSMF). The powers launched into the DCF are below 0 dBm for both the signal and the idler while the pump power is about 5 dBm.

The signal and idler waves are then amplified by EDFA2 and attenuated by VOA2. The signal launch power is measured at point P_{in} in **Figure 9**. The link consists of 105 km SSMF and a fiber Bragg-grating dispersion-compensating module (FBG-DCM) for the dispersion compensation. The total link loss is 30 dB, and the dispersion map is chosen for the optimum of efficient nonlinearity mitigation found for 10 GBd QPSK data.

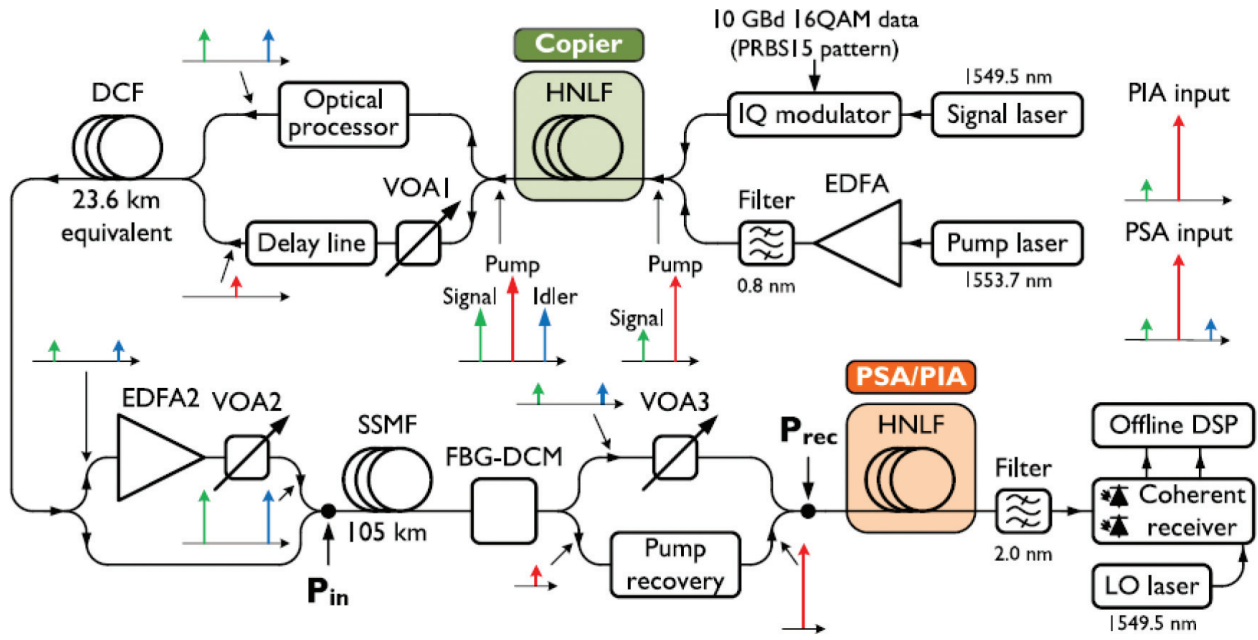


Figure 9. Experimental setup for simultaneous sensitivity improvement and nonlinearity mitigation in a 1 Gb/s 16QAM link. VOA: variable optical attenuator, FBG-DCM: fiber Bragg-grating dispersion-compensating module, PSA: phase-sensitive amplifier, PIA: phase-insensitive amplifier, LO: local oscillator, and DSP: digital signal processing.

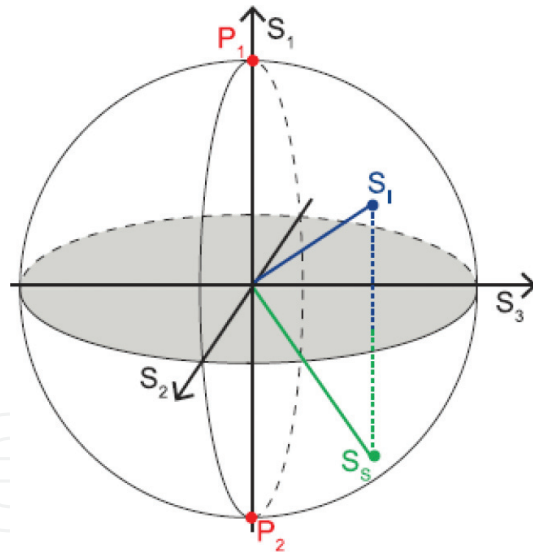


Figure 10. Polarization states on Poincaré sphere for vector PSA interaction. $S_{i,s}$ denote signal and idler Stokes vectors, and P_1 and P_2 are the pump Stokes vectors. S_s and S_i are mirrored in the plane (gray) normal to the pumps.

After the link, the pump wave is recovered by a hybrid EDFA/injection-locking system, before launched into the PIA/PSA. The pump recovery includes a PLL to stabilize the relative phase between the pump and the signal and idler. This is against thermal drift and acoustic noise introduced by splitting the pump and the signal and idler in different paths. The received signal power is varied using VOA3 and measured at point P_{rec} . Only the signal power is accounted when measuring launch power at P_{in} and received power at P_{rec} . The PIA/PSA

FOPA is implemented with a cascade of four HNLFs and provides 19 dB net gain in PS-mode and 13.5 dB net gain in PI mode.

The amplified signal is then filtered and passed to a preamplified coherent receiver, where it is mixed with a 300 kHz linewidth local oscillator laser at 1549.5 nm.

The same DD-LMS-based DSP is used to process the output from the numerical simulations with 16QAM. However, in this case, FFT-based frequency offset estimation in the DD-LMS loop is also adopted.

7.4. Polarization properties

In most applications of the copier-PSA the pump, signal and idler polarizations are aligned, and a scalar theory used. In a vector PSA, however, the polarization properties are important. The most common scheme for vector PSAs is the non-degenerate pump scheme, where the two pump waves are orthogonally polarized. An obvious question then is: what will the idler state of polarization (SOP) be, if the pumps and signal SOPs are given? The answer can be understood from the classical scatter-from-gratings picture.

Then the idler is given by two processes: pump 1 interferes with the signal and scatters pump 2 and vice versa. In terms of Jones vectors, the idler SOP will be given by

$$J_i = (J_s^H J_{p1}) J_{p2} + (J_s^H J_{p2}) J_{p1} \quad (25)$$

where J_{p1}, J_{p2}, J_s, J_i are the four Jones vectors and H denotes conjugate transpose. In matrix form, one can write $J_i^* = A^* J_s$, where the matrix is given by

$$A = J_{p1}^t J_{p2} + J_{p2}^t J_{p1} \quad (26)$$

The transfer matrix for vector PSA interaction then generalizes to

$$\begin{pmatrix} J_s \\ J_i^* \end{pmatrix}_{out} = \begin{pmatrix} \mu & vA \\ v^* A^* & \mu^* \end{pmatrix} \begin{pmatrix} J_s \\ J_i^* \end{pmatrix}_{in} \quad (27)$$

The geometrical interpretation of this scattering is shown on the Poincaré sphere (in Stokes space) in **Figure 10**. The orthogonally polarized pumps (antiparallel in Stokes space) are normal to a surface in which the signal and idler SOPs are mirrored. This generalizes a theory of Marhic [37], who considered the special case, $J_{p1} = (1, 0)t$ and $J_{p2} = (0, 1)t$. Note that the signal and idler are orthogonal to each other only when they are copolarized with the pumps, but not in the general case, which is a common misconception.

To conclude this subsection: for given orthogonal pumps and signal SOPs, the generated idler SOP will be the signal mirrored in plane normal to the pumps. This set of SOPs is generated in the copier. Then, for phase-sensitive interaction (coherent superposition) to take place, the signal, idler, and pump SOPs in to the PSA must be aligned as shown in **Figure 10**. Only the relative orientation matter, so any polarization mode dispersion (PMD) that changes the

relative SOPs of the four waves will reduce the phase-sensitive interaction, and must be compensated.

7.5. Transmission experiments

In practical implementations, the copier-PSA scheme is challenging as it requires full phase synchronization at each amplifier in the link, which require per-span dispersion compensation and phase tracking. Also, the polarization states need to be aligned. The pump needs to be transmitted together with the signal and idler, but must be selectively attenuated before sent in to the fiber. Then at the PSA, it must be recovered, amplified, and used as an intense pump in the PSA. This pump recovery scheme can be solved by injection locking. The first transmission experiment using a copier-PSA to implement these ideas was reported by Corcoran et al., who demonstrated transmission over a single 80 km span link [38].

In the same timeframe, Umeki et al. also reported transmission experiment using PSAs, but then using a periodically poled Lithium-Niobate PSA [39, 40]. That work is very different and not based on the copier-PSA idea. Rather the PSA is $\chi^{(2)}$ -based, which illustrates that this scheme can (in contrast with the copier-PSA scheme) only amplify a single quadrature. On the other hand, it does not require the bandwidth of the copropagating idler wave. This work was also extended to cover polarization division multiplexed transmission [41].

The copier-PSA scheme was extended to a full circulating loop experiment by Olsson [42] demonstrating transmission over 3400 km. It should be noted that the first recirculating loop experiment, based on high-gain PSAs and the copier-PSA configuration, increased transmission distance of around four times compared to a PIA-based link. The possibility of tolerating a nonlinear phase shift at a BER of 10^{-3} is 5.8 radians, making it to be one of the most nonlinear transmission experiments ever performed, while also demonstrating the potential of the PSA-based links.

The PSA also demonstrates the highest sensitivity reported in [43] for 10 Gb/s OOK data, reaching a sensitivity of -41.7 dBm for a BER = 10^{-9} .

8. Applications of parametric amplifier

8.1. Phase-sensitive amplification for phase and amplitude regeneration of differential phase-shift keyed signals

PSAs offer numerous advantages in optical communications. It offers stronger phase-matched gain and suppression of amplitude-to-phase noise conversion. Squeezing of optical phase through PSA can remove accumulated phase jitter. Different implementations of PSA were used for phase regeneration of both return-to-zero differential phase-shift keying and nonreturn-to-zero differential phase-shift keying data.

Ideally, a PSA can be configured to squeeze either the phase or the amplitude of a signal. For PSK systems, the former is chosen, and amplitude regeneration follows from the different

physical phenomenon of gain saturation. The orientation of the squeezing axis in phase regeneration should satisfy the synchronization of the pump and signal carrier phases, as shown in **Figure 11(a)**. A practical PSA operates as follows: the incident (noisy) signal is divided for processing and for the generation of pumps; owing to the carrier-suppressed nature of PSK formats, it is impossible to directly inject and lock a local laser to the signal frequency or to use straight forward phase-locked loops; and an optical carrier is derived from the signal through alternate means such as a decision-directed phase-locked loop.

An alternative method is to perform all optical carrier-phase and polarization recovery (CPPR). The process was recently demonstrated by using a PSA in an oscillator configuration. The resulting carrier can be used for injection locking (IL), as a local oscillator at the signal frequency. Owing to the PSA implementation, the resulting wave is amplified (by an NI-PSA) or modulated to produce sidebands (in a PSA based on FWM). The clock-recovery (CR) process can be implemented parallelly with CPPR. Phase stabilization is required when the signal and pump(s) are injected into the PSA. By properly orienting the axes, the maximum amplification is obtained.

A Sagnac PSA is configured in **Figure 12**. Ten gigabits per second RZ-DPSK data with 33% duty cycle and pattern length of at least $2^{11}-1$ is generated and divided into pump and signal

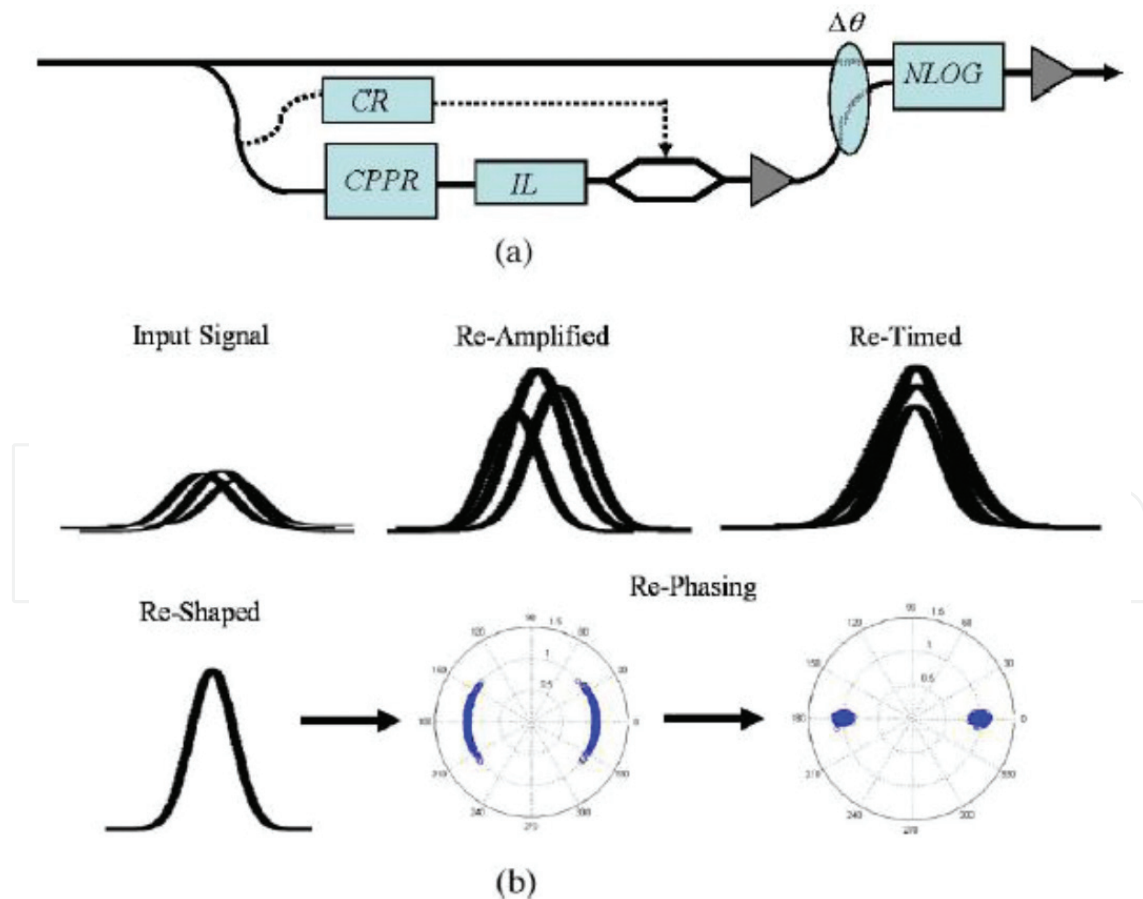


Figure 11. Regeneration of a DPSK signal. (a) Schematic of practical PSA. (b) Aspects of all-optical regeneration for DPSK. NLOG: nonlinear optical gate.

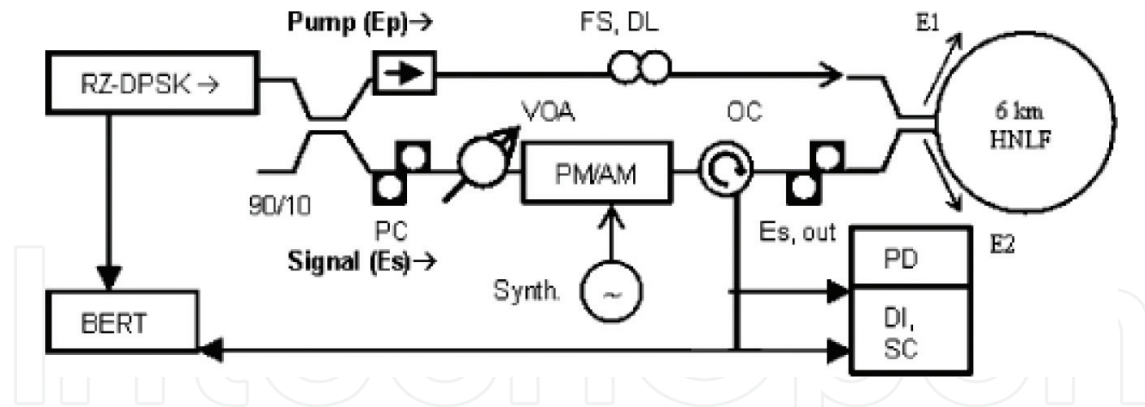


Figure 12. RZ-DPSK regeneration. FS: fiber stretcher; DL: delay line; OC: optical circulator; PC: polarization controller; DI: delay interferometer; SC: sampling oscilloscope; Synth: synthesizer; BERT: bit-error-ratio tester; PM/AM: noise adding phase and amplitude modulators.

paths. The use of a binary-phase-modulated pump can eliminate excess noise due to SBS. Different path lengths of the pump and signal ensure decorrelation of the PRBS data. The PN is quantified according to the maximum phase error, where $MPE = \max(\varphi_{n-1} - \varphi_n)$ is the maximum deviation of all detected differential phases from their original encoded values. An optical attenuator is used to adjust the pump to signal power ratio from 10 to 20 dB at the input. A free-space delay line in the pump path allows temporal alignment of the pump and signal pulses at the PSA input as well as a method for manually controlling the input phase difference. The input phase difference is stabilized by monitoring the signal gain and driving a fiber stretcher. The PSA comprises a 3 dB coupler and 6058 m HCF (not polarization maintaining) with a total insertion loss of 5 dB and effective nonlinear coefficient of 9.75/W/km. An intra-loop polarization controller is required to maximize the reflection of the pump and the transmission of the regenerated signal extracted by the optical circulator.

Several factors affect the ability of the PSA to simultaneously reduce phase and amplitude fluctuations. Performance is optimized when the average nonlinear phase shift $NLPS = \pi/2$ and the pump power is maximized, allowing the signal launch power to be minimized. In experiments, lower limits are placed on the launched signal power. Imperfections of the coupler in the PSA lead to leakage of pump. After PSA, the signal power significantly exceeds the leakage of the pump. Pump leakage increases when the intra-loop polarization controller is not adjusted properly. Due to thermal effect in the fiber, frequent adjustment of the controller is required, especially when the pumping power is changed. This problem is exacerbated when the fiber length is >6 km. And in this case, it is not polarization maintaining. Restrictions by these factors are easily removed through proper choice of components. Further restrictions resulting from pump wave imperfections is quantified in following results. To obtain the condition of $NLPS = \pi/2$, the phase-sensitive gain (PSG) at the signal port is monitored.

In **Figure 13**, light from a single tunable laser is divided into two paths for generations of pumps and a degraded signal. The signal is modulated with 10 Gb/s NRZ-DPSK data and the pattern length at least $2^{15}-1$ using a phase modulator. For regeneration experiments, nonlinear phase noise and amplitude fluctuations are simulated in previous experiments. Pump waves symmetrically around the signal frequency are generated with a carrier-suppressed return-to-

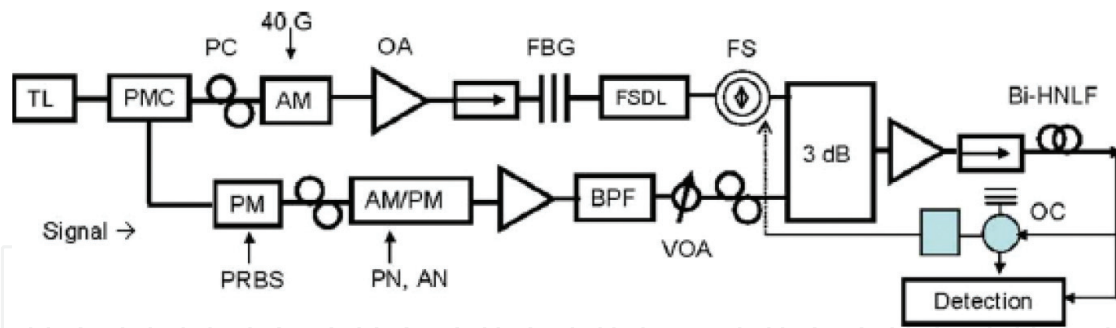


Figure 13. Experiment for NRZ-DPSK phase regeneration. TL: tunable laser; PMC: polarization maintaining coupler; OA: EDFA; FSDL: free-space delay line; FS: fiber stretcher; BPF: bandpass filter; Bi-HNLF: bismuth-oxide highly nonlinear fiber; and FBG: fiber Bragg grating.

zero (CSRZ) modulation. Experiments are performed with driving frequencies 20 and 40 GHz. The sideband separation is twice the driving frequency of the modulator, while power at the carrier frequency is typically 23 dB below that of either sideband. A FBG is used to further suppress light at the carrier frequency in the pump path to -38 dB and to minimize interference in the DPSK signal when the waves are mixed.

Both the pumps and signal are amplified by a high-power EDFA and launched into a bismuth-oxide-based optical fiber. Due to the short length, the total launch power is 31 dBm without the pump phase modulation to suppress SBS. This leads to the improvement of the performance since pump wave imperfections are minimized. The output signal is filtered and divided for feedback control and detection. Phase stabilization is achieved. The polarizations of input waves are aligned by scanning the signal phase (using a delay line) and simultaneously adjusting the polarization controller which also maximizes phase-sensitive gain. Careful adjustment allows polarization alignment but not gain an arbitrary polarization state: to obtain maximize performance, parallel linear polarizations should be adopted.

8.2. Parametric amplifier for squeezed state generation

A considerable degree of two mode broadband squeezing by combining two coherent strongly pumped single-pass type-I OPAs, which generate squeezed vacua in two orthogonal polarization modes is shown in **Figure 14** [44]. This creates a squeezed vacuum with the variance of some Stokes suppressed below the shot-noise level, which is determined by the mean number of photons. The latter, coinciding with the zeroth Stokes parameter S_0 , gives the variance of any Stokes of a coherent beam with the same mean photon number and with any polarization. This special two-mode squeezing is often termed polarization squeezing, and the state is called polarization-squeezed vacuum. This definition of polarization squeezing differs from the commonly used one [45], where the modulus of some Stokes observable mean value is $Var(S_i) < |\langle S_j \rangle| < Var(S_k)$, $i, j, k = 1, 2, 3$. This polarization squeezing is similar to quadrature squeezing rather than two mode squeezing. However, both are essentially non-classical.

In **Figure 14**, two 1 mm BBO crystals with the optical axes oriented in the vertical and horizontal planes are placed to induce the beam of a Nd:YAG laser third harmonic (wavelength $\lambda_p = 355$ nm).

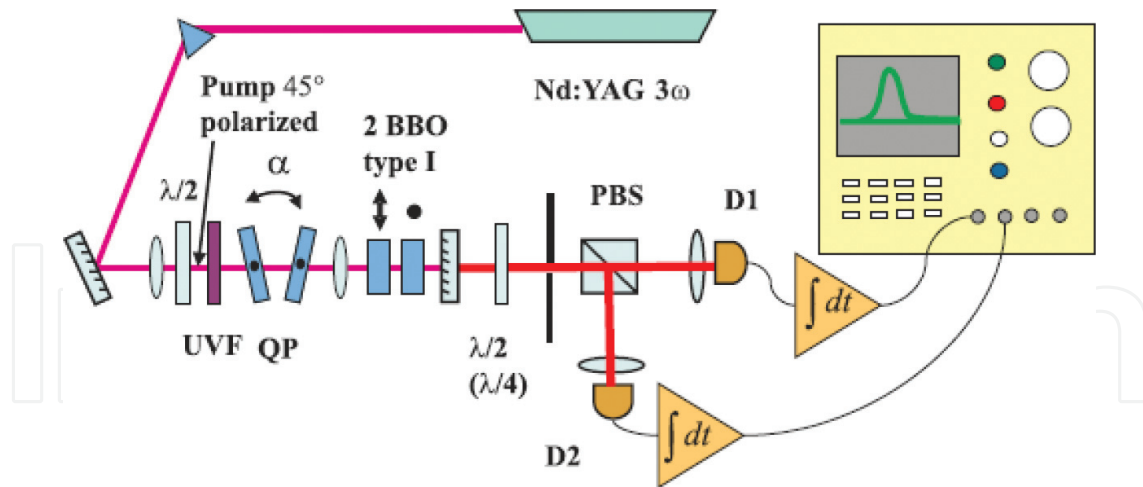


Figure 14. Experimental setup. UVF, UV filter; QP, quartz plates; PBS, polarizing beam splitter; and D1 and D2, detectors.

The fundamental and second-harmonic radiation of the laser is eliminated using a prism and a UV filter. The pump pulse width is 17 ps, the repetition rate is 1 kHz, and the mean power is up to 120 mW. The pump is focused into the crystals by either a lens with focal length 100 cm, which results in a beam waist of 70 μm , or with a telescope, providing a softer focusing (beam waist about 500 μm). Using a half wave plate (HWP), the pump polarization is aligned to be at 45° to the planes of the crystals' optical axes. The crystals are aligned for type-I collinear frequency-degenerate phase matching. After the crystals, the pump radiation is cut off by two dichroic mirrors with high reflection for the pump and 98.5% transmission for down-converted radiation.

The detection part includes a polarizing beam splitter, a HWP or a quarter wave plate (QWP), and two detectors and provides a standard Stokes measurement. With a HWP oriented at 22.5° , the difference of the detectors' signals corresponded to the second Stokes is S_2 , while with a QWP oriented at 45° , the same measurement is S_3 . All surfaces of the optical elements had a standard broadband antireflection coating. The angular spectrum of the detected light is restricted by an aperture to be 0.8° , and the wavelength range is only restricted by the phase matching and is 130 nm broad with the central wavelength 709 nm. The detectors are Hamamatsu S3883 *p-i-n* diodes and the pulsed charge-sensitive amplifiers are Amptek A250 and A275 chips, with peaking time 2.77 μs . They have a quantum efficiency of 90% and an electronic noise of 180 electrons/pulse rms. At the outputs, they produced pulses with the duration 8 μs and the amplitude proportional to the integral number of photons per light pulse. The phase between the states generated in the two crystals can be adjusted by tilting two quartz plates ($l_1 = 532 \mu\text{m}$ and $l_1 = 523 \mu\text{m}$), which are placed in the pump beam path and having the optical axes oriented vertically.

The output of the detectors is measured by means of an analog-digital card integrating the electronic pulses over time. The resulting integrals (up to the amplification factor A) coincide with the photon numbers incidented on the detectors during a light pulse. The amplification factors for detectors 1 and 2 are independently calibrated to be $A_1 = 9.96 \times 10^{-3}$ nV s/photon and $A_2 = 9.96 \times 10^{-3}$ nV s/photon. The difference between the amplification factors is eliminated numerically by multiplying the result of the measurement of detector 2 by a factor of

0.9–0.92, depending on the alignment. As a result, the output signals of the detectors are balanced to an accuracy of 0.1%. From the data set obtained from 30,000 pulses, the mean photon numbers per pulse are measured as well as the variances of the photon number difference and photon-number sum for the two detectors. Since the electronic noise is comparable to the shot-noise level, it has to be subtracted. The shot-noise is measured independently by using a shot-noise limited source and corresponds to a standard deviation of about 250 photons per pulse. The degree of two-mode squeezing is characterized by the noise reduction factor (NRF), the ratio of the photon-number difference variance to the mean photon-number sum.

9. Conclusion

By introducing the basic transmission theory of pump and signal lights in fibers, the principle of PA is interrupted which includes the properties of phase sensitivity, gain saturation, and noise. The systems for the parametric amplification, the Sagnac interferometer and directly generation in HNLF, are presented. Its applications for phase and amplitude regeneration of differential phase-shift keyed signals and for the generation of squeezed state are also introduced.

As the transmission system has to accommodate all types of modulation formats, the field of PA investigation attracts much attention again and it is worth paying more attention in the future.

Author details

Jing Huang

Address all correspondence to: huanggesheng@tom.com

Physics Department, South China University of Technology, Guangzhou, China

References

- [1] Karlsson M. Transmission systems with low noise phase-sensitive parametric amplifiers. *IEEE Journal of Lightwave Technology*. 2016;**34**:1411-1423. DOI: 10.1109/JLT.2015.2507866
- [2] Pocholle JP, Raffy J, Papuchon M, Desurvire E. Raman and four photon mixing amplification in single mode fibers. *Optical Engineering*. 1985;**24**:244600-244608. DOI: 10.1117/12.7973536
- [3] Bar-Joseph I, Friesem AA, Waarts RG, Yaffe HH. Parametric interaction of a modulated wave in a single-mode fiber. *Optics Letters*. 1986;**11**:534-536. DOI: 10.1364/OL.11.000534

- [4] Levenson JA, Grangier P, Abram I, Rivera T. Reduction of quantum noise in optical parametric amplification. *Journal of the Optical Society of America B*. 1993;**10**:2233-2238. DOI: 10.1364/JOSAB.10.002233
- [5] Marhic ME, Hsia CH, Jeong JM. Optical amplification in a nonlinear fibre interferometer. *Electronics Letters*. 1991;**27**:210-211. DOI: 10.1049/el:19910136
- [6] Imajuku W, Takada A, Yamabayashi Y. Low-noise amplification under the 3 dB noise figure in high-gain phase-sensitive fibre amplifier. *Electronics Letters*. 1999;**35**:1954-1955. DOI: 10.1049/el:19991343
- [7] Lundstrom C, Malik R, Gruner-Nielsen L, Corcoran B, Olsson SLI, Karlsson M, Andrekson PA. Fiber optic parametric amplifier with 10-dB net gain without pump dithering. *IEEE Photonics Technology Letters*. 2013;**25**:234-237. DOI: 10.1109/LPT.2012.2230160
- [8] Tang R, Lasri J, Devgan PS, Grigoryan V, Kumar P, Vasilyev M. Gain characteristics of a frequency nondegenerate phase-sensitive fiberoptic parametric amplifier with phase self-stabilized input. *Optics Express*. 2005;**13**:10483-10493. DOI: 10.1364/OPEX.13.010483
- [9] McKinstrie CJ, Radic S. Phase-sensitive amplification in a fiber. *Optics Express*. 2004;**12**:4973-4979. DOI: 10.1109/LEOSWT.2008.4444389
- [10] McKinstrie CJ, Yu M, Raymer MG, Radic S. Quantum noise properties of parametric processes. *Optics Express*. 2005;**13**:4986-5012. DOI: /10.1364/OPEX.13.004986
- [11] McKinstrie CJ, Raymer MG, Radic S, Vasilyev M. Quantum mechanics of phase-sensitive amplification in a fiber. *Optical Communications*. 2006;**257**:146-163. DOI: 10.1016/j.optcom.2005.07.023
- [12] Marhic ME, Kagi N, Chiang T-K, Kazovsky LG. Broadband fiber optical parametric amplifiers. *Optics Letters*. 1996;**21**:573-575. DOI: 10.1364/OL.21.000573
- [13] Marhic ME, Wong KK-Y, Kazovsky LG. Wide-band tuning of the gain spectra of one-pump fiber optical parametric amplifiers. *IEEE Journal of Selected Topics in Quantum Electronics*. 2004;**10**:1133-1141. DOI: 10.1109/JSTQE.2004.835298
- [14] Marhic ME. *Fiber Optical Parametric Amplifiers, Oscillators and Related Devices*. Cambridge, UK: Cambridge University Press; 2008. DOI: 10.1109/jstqe.2008.920032
- [15] Croussore K, Kim C, Li G. All-optical regeneration of differential phase-shift keying signals based on phase-sensitive amplification. *Optics Letters*. 2004;**29**:2357-2359. DOI: 10.1364/OL.29.002357
- [16] Croussore K, Kim I, Han Y, Kim C, Li G, Radic S. Demonstration of phase-regeneration of DPSK signals based on phase-sensitive amplification. *Optics Express*. 2005;**13**:3945-3950. DOI: 10.1364/OPEX.13.003945
- [17] Croussore K, Li G. Phase and amplitude regeneration of differential phase-shift keyed signals using phase-sensitive amplification. *IEEE Journal of Selected Topics in Quantum Electronics*. 2008;**14**:648-658. DOI: 10.1109/JSTQE.2007.915397

- [18] Karlsson M. Four-wave mixing in fibers with randomly varying zero dispersion wavelength. *Journal of the Optical Society of America B*. 1998;**15**:2269-2275. DOI: 10.1364/JOSAB.15.002269
- [19] Farahmand M, de Sterke M. Parametric amplification in presence of dispersion fluctuations. *Optics Express*. 2004;**12**:136-142. DOI: 10.1364/OPEX.12.000136
- [20] Ferrini G, Fsaifes I, Labidi T, Goldfarb F, Trep N, Bretenaker F. Symplectic approach to the amplification process in a nonlinear fiber: Role of signal-idler correlations and application to loss management. *Journal of the Optical Society of America B*. 2014;**31**:1627-1641. DOI: 10.1364/JOSAB.31.001627
- [21] Kakande J, Lundstrom C, Andrekson PA, Tong Z, Karlsson M, Petropoulos P, Parmigiani F, Richardson DJ. Detailed characterization of a fiber-optic parametric amplifier in phase-sensitive and phase-insensitive operation. *Optics Express*. 2010;**18**:4130-4137. DOI: 10.1364/OE.18.004130
- [22] Richter T, Corcoran B, Olsson SL, Lundstrom C, Karlsson M, Schubert C, Andrekson PA. Experimental characterization of a phase-sensitive four-mode fiber-optic parametric amplifier. In: *European Conf. Exhib. Optical Communication (ECOC)*. Amsterdam, Netherlands; 2012. Paper Th.1.F.1. DOI: 10.1364/ECEOC.2012.Th.1.F.1
- [23] McKinstrie CJ. Schmidt decompositions of parametric processes III: Simultaneous amplification and conversion. *Optics Express*. 2015;**23**:16949-16966. DOI: 10.1364/OE.23.016949
- [24] Kylemark P, Sunnerud H, Karlsson M, Andrekson PA. Semi-analytic saturation theory of fiber optical parametric amplifiers. *IEEE Journal of Lightwave Technology*. 2006;**24**:3471-3479. DOI: 10.1109/JLT.2006.880158
- [25] Tong Z, Lundstrom C, Andrekson PA, Karlsson M, Bogris A. Ultralow noise, broadband phase-sensitive optical amplifiers, and their applications. *IEEE Journal of Selected Topics in Quantum Electronics*. 2011;**18**:1016-1032. DOI: 10.1109/JSTQE.2011.2136330
- [26] Yamamoto Y, Haus H. Preparation, measurement and information capacity of optical quantum states. *Reviews of Modern Physics*. 1986;**58**:1001. DOI: 10.1103/RevModPhys.58.1001
- [27] Shirasaki M, Haus HA. Squeezing of pulses in a nonlinear interferometer. *Journal of the Optical Society of America B*. 1990;**7**:30-34. DOI: 10.1364/JOSAB.7.000030
- [28] Kylemark P, Ren J, Karlsson M, Radic S, McKinstrie CJ, Andrekson PA. Noise in dual-pumped fiber-optical parametric amplifiers: Theory and experiments. *IEEE Journal of Lightwave Technology*. 2007;**25**:2837-2846. DOI: 10.1109/JLT.2007.902098
- [29] Rudd JV, Law RJ, Luk TS, Cameron SM. High-power optical parametric chirped-pulse amplifier system with a 1.55 μm signal and a 1.064 μm pump. *Optics Letters*. 2005;**30**:1974-1976. DOI: 10.1364/OL.30.001974
- [30] Nicholson JW, Yablon AD, Westbrook PS, Feder KS, Yan MF. High power, single mode, all-fiber source of femtosecond pulses at 1550 nm and its use in supercontinuum generation. *Optics Express*. 2004;**12**:3025-3034. DOI: 10.1364/OPEX.12.003025

- [31] Yang S, Cheung KKY, Zhou Y, Wong KKY. Tunable single-longitudinal-mode fiber optical parametric oscillator. *Optics Letters*. 2010;**35**:481-483. DOI: 10.1364/OL.35.000481
- [32] Tang R, Devgan P, Voss PL, Grigoryan VS, Kumar P. In-line frequency—Nondegenerate phase-sensitive fiber-optical parametric amplifier. *IEEE Photonics Technology Letters*. 2005;**17**:1845-1847. DOI: 10.1109/LPT.2005.853226
- [33] Tong Z, Lundstrom C, Andrekson PA, McKinstrie CJ, Karlsson M, Blessing DJ, Tipsuwannakul E, Puttnam BJ, Toda H, Gruner-Nielsen L. Towards ultrasensitive optical links enabled by low-noise phase-sensitive amplifiers. *Nature Photonics*. 2011;**5**:430-436. DOI: 10.1038/nphoton.2011.79
- [34] McKinstrie CJ, Alic N, Karlsson M, Tong Z. Higher-capacity communication links based on two-mode phase-sensitive amplifiers. *Optics Express*. 2011;**19**:11977-11991. DOI: 10.1364/OE.19.011977
- [35] Liu X, Chraplyvy AR, Winzer PJ, Tkach RW, Chandrasekhar S. Phase-conjugated twin waves for communication beyond the Kerr nonlinearity limit. *Nature Photonics*. 2013;**7**:560-568. DOI: 10.1038/nphoton.2013.109
- [36] Olsson SLI, Corcoran B, Lundstrom C, Eriksson TA, Karlsson M, Andrekson PA. Phase-sensitive amplified transmission links for improved sensitivity and nonlinearity tolerance. *IEEE Journal of Lightwave Technology*. 2015;**33**:710-721. DOI: 10.1109/JLT.2014.2367096
- [37] Marhic ME. Polarization independence and phase-sensitive parametric amplification. *Journal of the Optical Society of America B*. 2011;**28**:2685-2689. DOI: 10.1364/JOSAB.28.002685
- [38] Corcoran B, Olsson SLI, Lundstrom C, Karlsson M, Andrekson PA. Phase-sensitive optical pre-amplifier implemented in an 80 km DQPSK link. *Optical Fiber Communication Conference*. Los Angeles, CA, USA; Mar. 2012. Paper PDP5A.4. DOI: 10.1364/OFC.2012.PDP5A.4
- [39] Umeki T, Asobe M, Takara H, Miyamoto Y, Takenouchi H. Multispan transmission using phase and amplitude regeneration in PPLN-based PSA. *Optics Express*. 2013;**21**:18170-18177. DOI: 10.1364/OE.21.018170
- [40] Umeki T, Asobe M, Takenouchi H. In-line phase sensitive amplifier based on PPLN waveguides. *Optics Express*. 2013;**21**:12077-12084. DOI: 10.1364/OE.21.012077
- [41] Umeki T, Kazama T, Tadanaga O, Enbutsu K, Asobe M, Miyamoto Y, Takenouchi H. PDM signal amplification using PPLN-based polarization-independent phase-sensitive amplifier. *IEEE Journal of Lightwave Technology*. 2015;**33**:1326-1332. DOI: 10.1109/JLT.2014.2385867
- [42] Olsson SLI, Lundström C, Karlsson M, Andrekson PA. Long haul (3465 km) transmission of a 10 GBd QPSK signal with low noise phase-sensitive in-line amplification. *European Conf. Exhib. Optical Communication, Cannes, France; Sep. 2014*. Paper PD.2.2. DOI: 10.1109/ECOC.2014.6964278

- [43] Malik R, Olsson SLI, Andrekson P, Lundström C, Karlsson M. Record-high sensitivity receiver using phase sensitive fiber optical parametric amplification. Optical Fiber Communication Conf.; San Francisco, CA, USA; Mar. 2014. Paper Th2A.54. DOI: 10.1364/OFC.2014.Th2A.54
- [44] Iskhakov T, Chekhova MV, Leuchs G. Generation and direct detection of broadband mesoscopic polarization-squeezed vacuum. Physics Review Letters. 2009;**102**:183602. DOI: 10.1103/PhysRevLett.102.183602
- [45] Heersink J, Gaber T, Lorenz S, Glöckl O, Korolkova N, Leuchs G. Polarization squeezing of intense pulses with a fiber-optic Sagnac interferometer. Physics Review A. 2003;**68**:013815. DOI: 10.1103/PhysRevA.68.013815

IntechOpen

